

Fatigue predictions in entire body of metallic structures using a limited number of vibration sensors

Costas Papadimitriou^{a,*}, Claus–Peter Fritzen^b, Peter Kraemer^b and Evangelos Ntotsios^a

^a *Department of Mechanical Engineering, University of Thessaly, Volos 38334, Greece*

^b *Institute of Mechanics and Control Engineering, University of Siegen, Siegen 57076, Germany*

* *Corresponding author. Tel: (+30) 24210 74006; Fax: (+30) 24210 74012; E-mail Address: costasp@uth.gr*

ABSTRACT

A methodology is proposed for estimating damage accumulation due to fatigue in the entire body of a metallic structure using output-only vibration measurements from a sensor network installed at a limited number of structural locations. Available frequency domain stochastic fatigue methods based on Palmgren-Miner damage rule, S-N fatigue curves on simple specimens subjected to constant amplitude loads, and Dirlik's probability distribution of the stress range are used to predict the expected fatigue damage accumulation of the structure in terms of the power spectral density (PSD) of the stress processes. The PSD of stresses at unmeasured locations are estimated from the response time history measurements available at the limited measured locations using Kalman filter and a dynamic model of the structure. The effectiveness and accuracy of the proposed formulation is demonstrated using a multi-degree-of-freedom spring-mass chain model arising from structures that consist of members with uniaxial stress states.

Keywords: Life prediction; Stochastic fatigue; Dynamic analysis; Spectral methods; Kalman filter

1. INTRODUCTION

Damage accumulation due to fatigue is an important safety-related issue in metallic structures. The linear Palmgren-Miner damage accumulation law [1-2] is often used to evaluate fatigue damage using available methods for cycle counting in variable amplitude measured stress response time histories and S-N curves obtained from laboratory experiments of simple specimens subjected to constant amplitude loads. The damage accumulation predictions are based on time histories measurements taken from a sensor network, consisting usually of strain rosettes, attached to the structure. Such predictions are only applicable for the locations where measurements are available. Due to practical and economical considerations, the number of sensors placed in a structure during operation is very limited and in most cases they do not cover all critical locations. Moreover, there are locations in the structure that one cannot install sensors such as submerged structures, underwater locations in offshore structures (oil refinery structures, offshore wind turbines, offshore steel jackets, etc.), heated structural components, internal points in solid structures, and non-approachable areas of large extended structures. Available fatigue prediction methods based only on measurements cannot be used to predict fatigue damage accumulation at such locations where measurements are not available. In order to infer damage due to fatigue at structural members where measurements are not available, one needs to predict the stress response time histories in these structural members using the available measurements obtained from the sensory system. In certain circumstances, such predictions can be possible if one combines the available measurements with the information obtained from a dynamic model (e.g. a finite element model) of the structure.

The methods for fatigue damage accumulation have been extended to treat the case that the excitations can be represented by a stochastic vector process with known correlation characteristics. Assuming that the structure behaves linearly and the excitation is modeled by a Gaussian stochastic vector process, the stress response at any point is a stochastic process that can be completely defined using the correlation characteristics of the stochastic excitations [3]. The fatigue damage accumulation at a structural location can then be computed using the characteristics of the stochastic processes of the components of the stress tensor at such a location. Methods for fatigue

damage accumulation for Gaussian narrow-band stress processes have been introduced using the Rayleigh approximation and extended to handle the case of wide-band Gaussian stress processes (e.g. [4-8]). A review and comparison of spectral methods for stochastic fatigue analysis based on wide-band Gaussian stochastic processes can be found in the work by Benasciutti and Tovo [9]. The formulations depend on the probability distribution of stress cycles corresponding to different stress levels in a stress response time history signal and the expected number of peaks per unit time of a stress process. Results for the expected fatigue damage accumulation predicted by the Palmgren-Miner linear law have been presented in terms of the spectral moments of the stress process which are readily obtained from the power spectral density of the stress components involved. For the important case of wide band processes encountered often in applications, the simulation-inspired Dirlik approximation [8] is widely used and is considered to be the most accurate formula for modeling the probability of stress cycles in terms of the spectral moments of the stress process. It is worth noting that the aforementioned frequency domain methods based on the stress power spectral densities or spectral moments use no information available from a sensor network. Instead, their predictive accuracy depends on the assumptions employed for the excitation characteristics and the models representing the structural behavior. However, these predictions fail to integrate the information provided by a network of sensors. The sensor information is expected to update and improve the fatigue predictions, making them consistent with the available measurements.

This work addresses the problem of estimating the expected damage accumulation or remaining lifetime due to fatigue in the entire body of a structure using output-only vibration measurements at a limited number of locations provided by a sensor network installed on the structure. The measurements may consist of response time histories such as e.g. strain, acceleration, velocity, displacement, etc. The expected fatigue damage accumulation in the entire structure is obtained by integrating (a) methods for predicting strain/stress response time histories and their correlation/spectral characteristics in the entire structure from output-only measured response time histories available at limited locations in the structure, and (b) frequency domain methods for estimating fatigue damage accumulation using the spectral characteristics of the predicted

strain/stress response time histories. The idea is to use Kalman filter [10] methods to predict the strain/stress response time histories at various locations within structural components using the measurements available at a limited number of locations. A schematic diagram of the fatigue lifetime prediction in the entire structure from limited number of sensors using Kalman filter, along with its use in inspection/maintenance decisions, is shown in Figure 1. Response time history measurements are collected from a limited number of points S_1, \dots, S_n , while stress time history predictions are made at any number of points P_1, \dots, P_m . For each prediction point P , the fatigue damage accumulation, or remaining fatigue lifetime T , is obtained by combining the information in the stress tensor time history $\sigma(t)$ for the point P , fatigue data sets (e.g. S-N-curves) and a damage accumulation model (e.g. Palmgren-Miner rule). Such predictions are restricted here to the case of linear structures and excitations that can be adequately represented by Gaussian stationary stochastic processes. The excitation time histories applied in the structure are considered to be unknown. However, for several operational conditions of structures, the excitation time histories can be considered to be samples of a Gaussian stationary stochastic process with unknown intensity and frequency content. The proposed methodology is thus applicable for the case where the responses can be modeled by Gaussian stationary processes and the measured response time histories are long enough so that they can be considered to be samples of stationary processes.

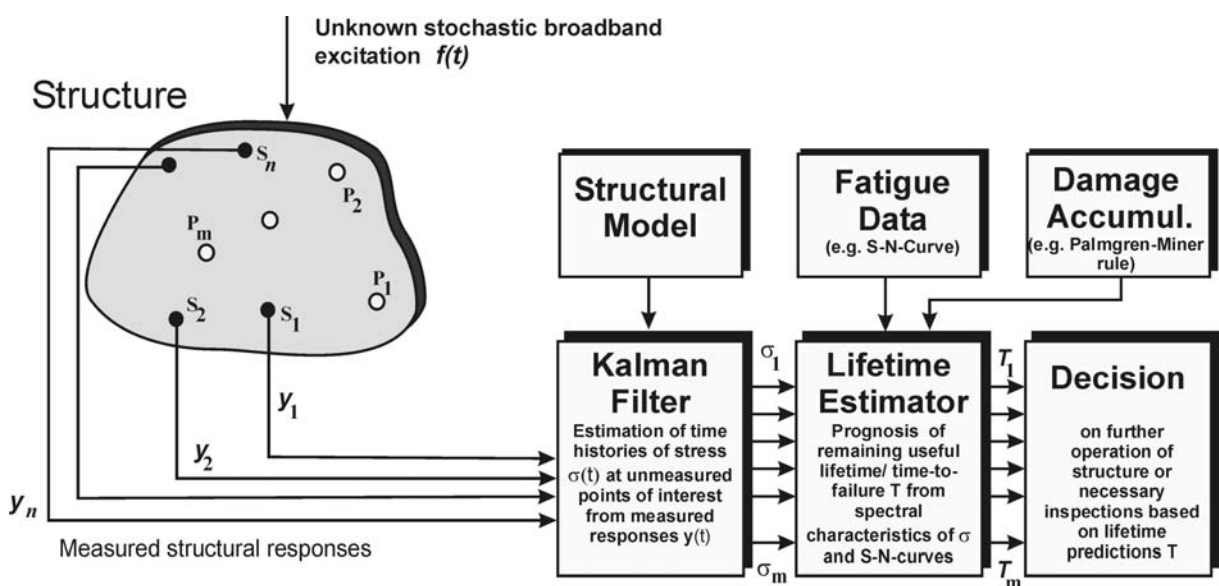


Fig. 1 Scheme of life-time prediction from a limited number of sensors using a Kalman Filter.

The objective of this work is to formulate the fatigue prediction problem, illustrate the methodology and point out its use in evaluating the damage accumulation in the entire structure from a limited number of vibration measurements. For this, the present approach is limited to uniaxial stress processes and simplified models of structures. The extension to multi-axial stress processes can be accomplished by using recent developments in frequency domain methods for stochastic fatigue based on spectral techniques [11-13]. These methods reduce the multi-axial stress state to an equivalent uniaxial stress state that can be treated by available fatigue estimation techniques based on spectral methods. In addition, extension to non-Gaussian stress processes, known to significantly affect fatigue life predictions [5,14], can also be accomplished by using recent approximations for the probability distribution of the stress cycles [15] in terms also of the higher moments of the stress process such as skewness and kurtosis.

This work is organized as follows. In Section 2, the frequency domain formulation for predicting damage due to fatigue in structural elements subjected to uniaxial stress state in linear structures under Gaussian stochastic excitations is reviewed. The formulation is applicable to Gaussian wide-band stress processes, often encountered in engineering applications, and damage accumulation due to fatigue depends on the spectral moments of the power spectral densities of the stress process at a location of a structure. Section 3 presents the formulation for predicting the strain/stress response time histories and the associated power spectral densities at all desirable locations of the structure using Kalman filter and the measured time histories at a limited number of locations in the structure. For this, first the state space formulation of the equations governing the vibrations of a structure is briefly summarized in Section 3.1. Using the discrete-time formulation of the state space approach, the Kalman filter approach for estimating the power spectral densities of the stresses in the entire body of the structure is presented in Section 3.2 and 3.3. The approach considers that the unmeasured excitations can be represented by Gaussian stationary stochastic processes. Finally, Section 4 demonstrates the effectiveness of the proposed methodology using a chain-like mass-spring multi-degree-of-freedom (MDOF) structure and “measured” data that are simulated from various types of excitations, including white noise and filtered white noise excitations. Conclusions are summarized in Section 5.

2. FREQUENCY DOMAIN METHOD FOR FATIGUE ESTIMATION BASED ON SPECTRAL MOMENTS

The Palmgren-Miner rule [1-2] is commonly used to predict the damage accumulation due to fatigue. According to this rule, a linear damage accumulation law at a point in the structure subjected to variable amplitude stress time history is defined by the formula

$$D = \sum_i^m \frac{n_i}{N_i} \quad (1)$$

where n_i is the number of cycles at a stress level σ_i , N_i is the number of cycles required for failure at a stress level σ_i , and m is the number of stress levels identified in a stress time history at the corresponding structural point. Available S-N fatigue curves, obtained from laboratory experiments on simple specimens that are subjected to constant amplitude loads, are used to describe the number of cycles N_i required for failure in terms of the stress level σ_i . The number of cycles n_i at a stress level σ_i are usually obtained using available stress cycle counting methods, provided that the stress time histories are available through measurements. Alternatively, for the cases where the stress response time histories are not available from measurements, frequency domain methods based on spectral moments (e.g. [5,9]) can be used to predict the expected damage due to fatigue using the linear damage law (1). The methodology assumes that the power spectral density of the stress process at a structural location is available. For linear systems excited by time-varying loads that can be modeled by stationary stochastic processes, these power spectral densities can be straightforwardly computed using available random vibration results [3].

The following section outlines such a frequency domain methodology based on spectral moments for fatigue estimation for structural members subjected to uniaxial stress state. For multi-axial stress states one can apply available methods [11-13] to extend the applicability of the present methodology. Let $\sigma(t)$ be the uni-axial stress at a point in a structural element. The stress is considered to be a stationary Gaussian stochastic process. This is the case encountered in linear structures that are subjected to stationary Gaussian stochastic processes. Let $S_\sigma(\omega)$ be the power

spectral density of the stationary Gaussian stochastic stress process $\sigma(t)$ of the uni-axial stress at a structural location and

$$\lambda_j = \int_{-\infty}^{\infty} |\omega|^j S_{\sigma}(\omega) d\omega \quad (2)$$

be the spectral moments of the process. Using frequency domain methods for fatigue estimation under stochastic excitations and the continuous version of the damage accumulation law (1), the expected fatigue damage accumulation for a uni-axial stochastic stress process is given by [9]

$$E[D] = \int_0^{\infty} \frac{n(\sigma)}{N(\sigma)} d\sigma = c^{-1} T E[P] \int_0^{\infty} \sigma^{\alpha} p(\sigma) d\sigma \quad (3)$$

where $n(\sigma) = T E[P] p(\sigma) d\sigma$ is the number of cycles at stress levels within the stress interval $[\sigma, \sigma + d\sigma]$, $p(\sigma)$ is the probability distribution of the stress levels,

$$N(\sigma) = c \sigma^{-\alpha} \quad (4)$$

is the number of cycles for failure that correspond to a specific constant amplitude stress level σ obtained from available S-N curves, $E[P]$ is the expected number of peaks per unit time for the stress process, and T the period of observation. The parameters c and α are constants obtained from fatigue test experiments and depend on the material and the type of the test specimen.

The expected time of failure due to fatigue (fatigue lifetime) T_{life} corresponds to a critical expected damage value $E[D] = D_{cr}$ which is often set equal to unity ($D_{cr} = 1$). Using (3), the fatigue lifetime is given by

$$T_{life} = \frac{D_{cr}}{\bar{D}} \quad (5)$$

where \bar{D} is the expected damage rate given by

$$\bar{D} = c^{-1} E[P] \int_0^{\infty} \sigma^{\alpha} p(\sigma) d\sigma \quad (6)$$

For Gaussian stochastic stress processes, the probability distribution of the stress range $\Delta\sigma = 2\sigma$, taken to be twice the random amplitude at stress level within $[\sigma, \sigma + d\sigma]$ in a stress process, is given by the Dirlik formula [8,16-17] as

$$p(\Delta\sigma) = \frac{1}{2\sqrt{\lambda_0}} \left[\frac{d_1}{h} e^{-\frac{\Delta\sigma}{2h\sqrt{\lambda_0}}} + \frac{d_2\Delta\sigma}{2r^2\sqrt{\lambda_0}} e^{-\frac{(\Delta\sigma)^2}{8r^2\lambda_0}} + \frac{d_3\Delta\sigma}{2\sqrt{\lambda_0}} e^{-\frac{(\Delta\sigma)^2}{8\lambda_0}} \right] \quad (7)$$

where d_1, d_2, d_3, h and r are specific algebraic functions of the spectral moments $\lambda_0, \lambda_1, \lambda_2, \lambda_4$, given by

$$d_1 = \frac{2(x_m - \alpha_2^2)}{1 + \alpha_2^2}, \quad d_2 = \frac{1 - \alpha_2 - d_1 + d_1^2}{1 - r}, \quad d_3 = 1 - d_1 - d_2 \quad (8)$$

$$h = \frac{1.25(\alpha_2 - d_3 - d_2r)}{d_1}, \quad r = \frac{\alpha_2 - x_m - d_1^2}{1 - \alpha_2 - d_1 + d_1^2} \quad (9)$$

$$x_m = \frac{\lambda_1}{\lambda_0} \left[\frac{\lambda_2}{\lambda_4} \right]^{\frac{1}{2}} = \alpha_1\alpha_2, \quad \alpha_1 = \frac{\lambda_1}{\sqrt{\lambda_0\lambda_2}}, \quad \alpha_2 = \frac{\lambda_2}{\sqrt{\lambda_0\lambda_4}} \quad (10)$$

This is a semi-empirical probability density which is a mixture of one exponential and two Rayleigh distributions. It has been derived by fitting the shape of a rain-flow range distribution via minimizing the normalized error between the rain-flow ranges and the above density model. The spectral moments $\lambda_0, \lambda_1, \lambda_2, \lambda_4$ constitute a base for the construction of the approximate closed-form Dirlik formula for the probability density of the stress range. The Dirlik formula constitutes an extension of the Rayleigh distribution to non-narrow band processes. It is widely used for fatigue crack estimation under wide-band Gaussian stationary applied stress. Extension to non-Gaussian stress processes requiring the skewness and kurtosis of the stress process are available in the work by Wang and Sun [15].

Using results from random vibration theory, the expected number of cycles $E[P]$ per second for a stochastic process is given by the spectral moments of the process in the form

$$E[P] = \frac{1}{2\pi} \sqrt{\frac{\lambda_4}{\lambda_2}} \quad (11)$$

Starting with (6) and noting that $p(\sigma) = p(\Delta\sigma)/2 = p(2\sigma)/2$, then substituting (11) and the Dirlik formula (7) into (6) and finally carrying out the integration in (6) analytically, the expected damage rate simplifies to [9]

$$\bar{D} = (8\pi c)^{-1} \sqrt{\frac{\lambda_4}{\lambda_2}} \lambda_0^{\alpha/2} \left[d_1 h^\alpha \Gamma(1+\alpha) + 2^{\alpha/2} \Gamma\left(1+\frac{\alpha}{2}\right) (d_2 |r|^a + d_3) \right] \quad (12)$$

where d_1 , d_2 , d_3 , h and r are defined in (8)-(10).

It is clear from the aforementioned formulation and equations (5) and (12) that the expected fatigue damage rate \bar{D} and, consequently, the fatigue accumulation during a time interval T or the fatigue lifetime T_{life} at a point in the structure depends only on the spectral moments λ_i , $i = 0, 1, 2, 4$, of the stress process $\sigma(t)$. Using the definition of the spectral moments in (2), the spectral moments and the fatigue predictions at a point of a structure eventually depend only on the power spectral density $S_\sigma(\omega)$ of the stress process $\sigma(t)$.

The power spectral densities of the stress response processes at a point can be calculated from measurements, provided that these measurements are long enough to be considered stationary. However, there is a limited number of points that can be instrumented in the structure. For the points where measurements are not available, one has to make predictions of the stress process and subsequently the power spectral density of the stress process at a location, given the measurements at other locations. This issue of predicting the power spectral densities of the stress processes in the entire body of the structure using measurements at limited locations is addressed at the next Section 3. Once these measurements and predictions of the stresses are estimated at measured and unmeasured locations, the power spectral densities and the corresponding damage accumulation or lifetime due to fatigue are obtained, using (5) and (12), everywhere in the structure. In this way, fatigue damage accumulation maps for the entire structure are constructed from the limited number of ambient vibration measurements.

3 RESPONSE PREDICTIONS IN THE ENTIRE STRUCTURE USING AMBIENT VIBRATION MEASUREMENTS

The objective of this section is to predict the stress response at all points in a structure using the measurements at a limited number of locations. This is achieved using an approach that is outlined

in the next two subsection based on the commonly used Kalman filter method [10] for full state estimation of a linear system using limited number of measurements.

3.1 Equations of Motion and State Space Formulation

Consider the dynamic response of a linear structural system subjected to deterministic and random excitations. Using a spatial discretization method, such as finite element analysis, the equations of motion are given by the following set of N second order differential equations

$$M \ddot{\underline{q}}(t) + C \dot{\underline{q}}(t) + K \underline{q}(t) = L_u \underline{u}(t) + L_w \underline{w}(t) \quad (13)$$

where $\underline{q}(t) \in \mathbb{R}^{N \times 1}$ is the displacement vector, M , C and $K \in \mathbb{R}^{N \times N}$ are respectively the mass, damping and stiffness matrices, $\underline{u}(t) \in \mathbb{R}^{N_{u,in} \times 1}$ and $\underline{w}(t) \in \mathbb{R}^{N_{w,in} \times 1}$ are the applied deterministic and stochastic excitation vectors of dimension $N_{u,in}$ and $N_{w,in}$, respectively, and $L_u \in \mathbb{R}^{N \times N_{u,in}}$ and $L_w \in \mathbb{R}^{N \times N_{w,in}}$ are matrices comprised of zeros and ones that map the $N_{u,in}$ and $N_{w,in}$ deterministic and stochastic excitation loads to the N output DOFs. Throughout the analysis, it is assumed that the system matrices M , C and K are symmetric. Let $\underline{y}(t) \in \mathbb{R}^{N_{meas}}$ be the vector that collects all measurements at different locations of the structure at time t . These measurements are generally collected from sensors such as accelerometers, strain gauges, etc. For convenience and without loss of generality, it is assumed in the analysis that sensors placed in the structure measure the strains.

Introducing the state vector $\underline{x}^T = [\underline{q}^T \quad \dot{\underline{q}}^T] \in \mathbb{R}^{1 \times 2N}$, the equation of motion can be written in the state space form

$$\dot{\underline{x}} = A_c \underline{x} + B_c \underline{u}(t) + G_c \underline{w}(t) \quad (14)$$

while the measured output vector $\underline{y}(t)$ is given by the observation equation

$$\underline{y}(t) = H \underline{x} + D \underline{u}(t) \quad (15)$$

where the state transition matrix A_c , and the matrices B_c and G_c are given by

$$A_c = \begin{bmatrix} 0 & I \\ -M^{-1}K & -M^{-1}C \end{bmatrix} \in \mathbb{R}^{2N \times 2N} \quad (16)$$

$$B_c = \begin{bmatrix} 0 \\ -M^{-1}L_u \end{bmatrix} \in \mathbb{R}^{2N \times N_{u,in}} \quad \text{and} \quad G_c = \begin{bmatrix} 0 \\ -M^{-1}L_w \end{bmatrix} \in \mathbb{R}^{2N \times N_{w,in}} \quad (17)$$

respectively, $H \in \mathbb{R}^{N_{meas} \times 2N}$ is the observation matrix and $D = 0 \in \mathbb{R}^{N_{meas} \times 2N_{u,in}}$ for strain measurements.

3.2 Kalman Filter Approach

Since measurements are available in digitized form, the presentation of the Kalman filter is next given in discrete time. Using the sampling rate $1/\Delta t$, the discrete-time state space model corresponding to (14) and (15) is

$$\underline{x}_k = A\underline{x}_{k-1} + B\underline{u}_{k-1} + G\underline{w}_{k-1} \quad (18)$$

$$\underline{y}_k = H\underline{x}_k + D\underline{u}_k + \underline{v}_k \quad (19)$$

where $\underline{x}_k = \underline{x}(k\Delta t)$ and $\underline{y}_k = \underline{y}(k\Delta t)$, $k = 1, \dots, N_s$, are the digitized state and output vectors, and $A = e^{A_c \Delta t}$ is the state transition matrix for the discrete formulation. The random variables w_k and v_k represent the stochastic excitation and the measurement noise, respectively. They are assumed to be independent, white and following normal probability distributions $p(w_k) \sim N(0, Q)$ and $p(v_k) \sim N(0, R)$, where Q and R are the stochastic excitation and the measurement noise covariances assumed to be constant, independent of time.

Kalman filter is used to estimate the state $\hat{\underline{x}}_k$ of the system described by (18) using the measurements in the vector \underline{y}_k in (19). Specifically, in the prediction step, an apriori state estimate $\hat{\underline{x}}_k^-$ of the state vector \underline{x}_k of the system is estimated from equation [18-19]

$$\hat{\underline{x}}_k^- = A\hat{\underline{x}}_{k-1} + B\underline{u}_{k-1} \quad (20)$$

In the correction step, the measured value \underline{y}_k is used to calculate a posteriori state estimate $\hat{\underline{x}}_k$, weighting the measured and estimated signals by the Kalman filter gain factor K_k . This is formulated by the equation

$$\hat{\underline{x}}_k = \hat{\underline{x}}_k^- + K_k[\underline{y}_k - H\hat{\underline{x}}_k^- - D\underline{u}_k] \quad (21)$$

where the Kalman gain factor is given by

$$K_k = P_k H^T [HP_k H^T + R]^{-1} \quad (22)$$

and, for steady state response, the error covariance matrix $P_k \equiv P = E[e_k^-(e_k^-)^T]$, where $e_k^- = \underline{x} - \hat{\underline{x}}_k^-$ is the a priori error estimate, satisfies the discrete time Riccati equation:

$$P = APA^T - APH^T (HPH^T + R)^{-1} HPA^T + GQG^T \quad (23)$$

Let $\underline{\sigma}_k$ be a vector containing the digitized stresses at time $t = k\Delta t$ at various locations of the structure. Using structural mechanics theory, these stresses in the vector $\underline{\sigma}_k$ are related to the state vector through a linear transformation $\underline{\sigma}_k = \Sigma \underline{x}_k$, where Σ is the transformation matrix that associates the state vector to the desired stresses in the entire structure. Consequently, an estimate of the stresses $\hat{\underline{\sigma}}_k$ is related to the state vector estimate $\hat{\underline{x}}_k$ through the transformation:

$$\hat{\underline{\sigma}}_k = \Sigma \hat{\underline{x}}_k \quad (24)$$

Herein, the response prediction vector $\underline{\sigma}_k$ is restricted to stresses at elements subjected to uniaxial stress states required in lifetime fatigue estimation as described in Section 2.

Using the definition of the cross power spectral density (CPSD), the Kalman filter equations (20) and (21), the fact that $B = 0$ in (20) for the case of stochastic excitations and $D = 0$ in (21) for strain measurements, the CPSD $S_{\hat{\underline{\sigma}}_k}(\omega)$ of the stress response vector $\hat{\underline{\sigma}}_k$ can readily be obtained with respect to the CPSD $S_{\underline{y}_k}(\omega)$ of the measurement vector \underline{y}_k in the form

$$S_{\hat{\underline{\sigma}}_k}(\omega) = \Sigma S_{\underline{x}}(\omega) \Sigma^T = \Sigma E^{-1}(j\omega) K S_{\underline{y}_k}(\omega) K^T E^{-T}(j\omega) \Sigma^T \quad (25)$$

where $E(j\omega)$ is the matrix given by

$$E(j\omega) = I e^{j\omega\Delta t} - (I - KH)A \quad (26)$$

and I is the identity matrix. Equation (25) relates the power spectral densities of the components of the stress vector $\underline{\sigma}_k$ at various structural locations with the power spectral densities of the measured quantities involved in \underline{y}_k available at the limited number of measured locations. This relation depends on the model (e.g. a finite element model) used to represent the behavior of the

structure and the assumption that the excitation vector is broad-band so that the excitations can be modeled by zero-mean stationary white noise processes with spectral density described by $E[\underline{w}_k \underline{w}_l^T] = Q \delta_{kl}$, where δ_{kl} is the Kronecker delta.

It should be noted that in order to apply (23), an estimate of the zero-lag covariance matrix R of the measurement noise and the zero-lag covariance matrix Q of the unknown input stochastic vector process has to be provided. The values of the covariance matrix R which have to be chosen, affects the estimates of the cross power spectral density matrix $S_{\hat{e}}(\omega)$ in (25). However, an optimal estimate of the covariance matrix Q can be obtained using the strain measurements $\underline{y}(t)$ and the relation $Q_{yy} \equiv Q_{yy}(Q)$ between the covariance matrix Q_{yy} of the measurement vector $\underline{y}(t)$ and the covariance matrix Q of the excitation process. Using (19) with $D=0$ for strain measurements, this relation is given by

$$Q_{yy} = H Q_{xx} H^T \quad (27)$$

where Q_{xx} is given by the discrete time Lyapunov equation for the system (18) in the form

$$A Q_{xx} A^T - Q_{xx} + G Q G^T = 0 \quad (28)$$

The optimal values of the entries of the covariance matrix Q can be obtained by minimizing the difference between the covariance matrix $Q_{yy} \equiv Q_{yy}(Q)$ predicted by the linear model given Q and the covariance matrix $\hat{Q}_{yy} = (1/N_s) \sum_{k=1}^{N_s} \underline{y}_k \underline{y}_k^T$ obtained from the measurements in \underline{y}_k , $k = 1, \dots, N_s$. That is, the optimal value Q_{opt} is obtained by minimizing the objective function

$$J(Q) = tr \| Q_{yy}(Q) - \hat{Q}_{yy} \|^2 / tr \| \hat{Q}_{yy} \|^2 \quad (29)$$

with respect to the elements in Q . The optimal value Q_{opt} of Q is then substituted in (23) to completely define the Riccati equation (23). The solution P of the Riccati equation is substituted in (22) in order to find K which is needed in (25). It should be noted that the optimal estimate of Q , as described above, assumes that the stochastic excitations in the vector process \underline{w}_k are sufficiently broadband so that they can be adequately approximated by white noise processes.

3.3 Estimation of Power Spectral Densities of Stresses

The cross power spectral density matrix $S_{\underline{y}}(\omega)$ of the sampled measurement vector \underline{y}_k , involved in (25), can be obtained using available signal processing techniques such as the Welch technique [20-21]. Once $S_{\underline{y}}(\omega)$ has been estimated from the measurements, equation (25) can be used to estimate the cross power spectral density $S_{\underline{\hat{\sigma}}_k}(\omega)$ of the stress response vector $\underline{\hat{\sigma}}_k$.

Alternatively, the PSD $S_{\underline{\hat{\sigma}}_k}(\omega)$ of the stress response vector $\underline{\hat{\sigma}}_k$ can be obtained by using equations (20) and (21) for the Kalman filter to provide estimates $\underline{\hat{x}}_k$ of the system state vector which are then used in equations (24) to estimate the stress vector $\underline{\hat{\sigma}}_k$. Finally, available signal processing techniques such as the Welch technique are used to compute the PSD $S_{\underline{\hat{\sigma}}_k}(\omega)$ from the sampled stress response vector $\underline{\hat{\sigma}}_k$. The length of the sampled time history should be sufficient large in order for the estimates to be accurate.

Once the cross power spectral density matrix $S_{\underline{\hat{\sigma}}_k}(\omega)$ of the stress vector process $\underline{\hat{\sigma}}_k$ containing the stresses at all desirable structural locations is obtained, the diagonal elements $diag[S_{\underline{\hat{\sigma}}_k}(\omega)]$ of the matrix $S_{\underline{\hat{\sigma}}_k}(\omega)$ contain the power spectral density estimates required for fatigue predictions at these structural location using equations (2), (5) and (12).

4 APPLICATION ON SPRING-MASS CHAIN-LIKE MODEL

The applicability and effectiveness of the methodology is illustrated using simulated “measurements” from a simple class of N -DOF spring mass chain-like model fixed at the two ends as shown in Figure 2. The model is used to represent a structure consisting of a series of bar and body elements as shown in Figure 3. The structure consists of N bodies with the i -th body having mass m_i . The $i-1$ and the i bodies are connected by elastic bar elements which provide the stiffness to the system. The number of bar (or spring) elements of the chain model is $N+1$. The material of the bar elements is considered to be steel. For steel bar elements, the values of the fatigue constants in equation (4) are taken to be $c = 4.06 \times 10^{88}$ and $a = 9.82$. The i -th bar

element has length L_i , cross-sectional area A_i and modulus of elasticity E_i . For simplicity, each bar element is represented by a spring element with stiffness $k_i = E_i A_i / L_i$ as shown in Figure 2. Also, the nodal mass m_i in Figure 2 includes the effect of the i body mass and the lumped mass arising from the bar elements connected to node i . The i component $q_i(t)$ of the vector $\underline{q}(t)$ corresponds to the displacement of the node i of the model. The system is subjected to an unmeasured excitation applied at node ρ . For the selected structure, the stress state at critical bar locations is uniaxial so that the fatigue prediction methodology can be directly applied.

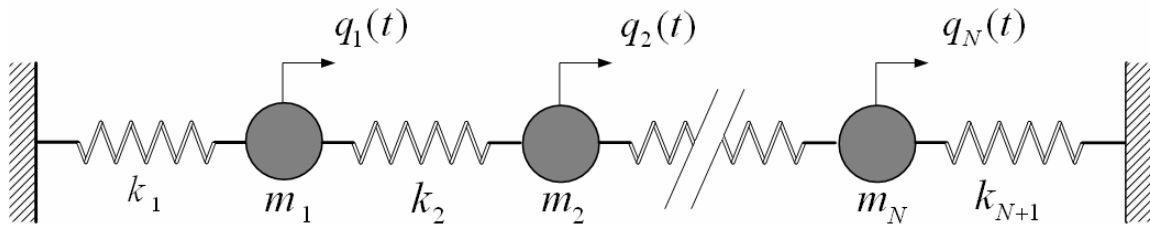


Fig. 2 N -DOF spring mass chain-like model.

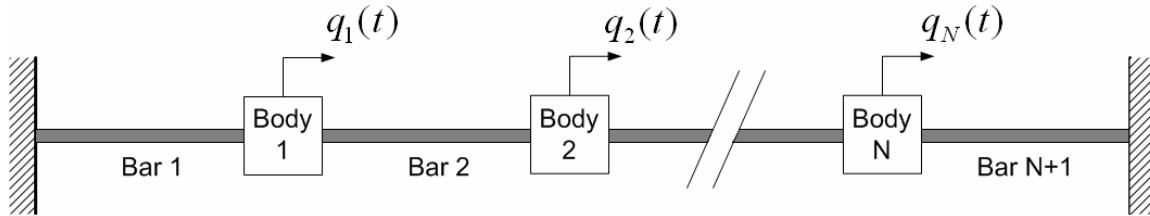


Fig. 3 Structure consisting of a series of N masses and $N + 1$ bar elements.

Fatigue predictions from the Kalman filter (KF) methodology are based on a nominal model of the structure that corresponds to nominal stiffness values $k_i = k_{0,i}$. The measurements that are collected from the actual structure are generated from a reference model introduced to simulate the actual behavior of the structure. In order to study the effects of the model error on the accuracy of the Kalman filter method for fatigue predictions, the reference model is selected to be different from the nominal model. Specifically, the reference model corresponds to the model shown in Figure 2 with stiffness values perturbed from the nominal stiffness values according to the

expression $k_i = k_{0,i}(1 + n_i)$, where $k_{0,i}$ are the nominal values used in KF-based fatigue predictions and $n_i \sim N(0, s_i^2)$ are samples from a zero mean normal distribution with variance s_i^2 . The standard deviation s_i of the perturbed terms controls the size of the model error and reflects the differences observed in real applications between the predictions from a model of a structure and the actual behavior of the structure.

The measurements are assumed to be strain measurements. These measurements are simulated from the reference model of the structure using two types of excitations, referred to as Type I and Type II excitations. Type I excitations are assumed to be samples of a Gaussian white noise process, thus providing good approximation to an excitation whenever its correlation time is sufficiently small compared to the system time constants. In this case the excitation vector $\underline{u}(t)$ is modeled by samples generated by a Gaussian stationary white noise vector process $\underline{n}(t)$ with constant spectral density matrix $S_{\underline{u}} = S_0$. Type II excitations are assumed to be samples of a uni-modal filtered white noise excitation with characteristics given by the second order filter equation

$$\ddot{q}_f(t) + 2\zeta_f \omega_f \dot{q}_f(t) + \omega_f^2 q_f(t) = n(t) \quad (30)$$

$$u(t) = \ddot{q}_f(t) = -2\zeta_f \omega_f \dot{q}_f(t) - \omega_f^2 q_f(t) + n(t) \quad (31)$$

The characteristics of the excitation depend on the values of the filter parameters: the dominant frequency ω_f and the damping ratio ζ_f . The value of the power spectral density S_0 of the Gaussian stationary white noise process $n(t)$ controls the intensity of the excitation samples $u(t)$ generated by the second-order filter.

For type I excitation, the discrete state space formulation of the equations of motion for the reference model is used to simulated response time history data as well as compute estimates of the covariance responses and the power spectral density of the responses using the white noise excitation $n(t)$ applied at node ρ . For type II excitation, the responses from the reference model can readily be obtained by a discrete state space formulation of an augmented system which consists of the equations of motion (13) and the filter equations (30)-(31) excited by the white noise

process $n(t)$. In this augmented system, the system states includes the states of the original system in (14) and the filter states arising from (30). For both excitation types, the strain and stress response time histories $\underline{\varepsilon}_k$ and $\underline{\sigma}_k$, respectively, are simulated at all bar elements using the discrete state space formulation. The time discretization step used in simulating the sampled data is $\Delta t = 0.5 \times 10^{-3}$. The simulated strain and stress response time histories are the reference stress response time histories that are considered to be the exact stress response time histories for the excitations used. These response time histories and the corresponding power spectral densities are also used with the fatigue methodology in Section 2 to compute the damage accumulation and lifetime of the entire body of the structure due to fatigue. Such predictions constitute the reference (exact) predictions against which the predictions from the proposed Kalman filter approach should be compared to for assessing the accuracy of the proposed methodology.

For convenience, the set o is introduced that contains the bar element numbers where the strains are measured. The measured strain response time histories $\underline{y}_k = \underline{\varepsilon}_k^{(o)}$ are the components of the reference response time history vector $\underline{\varepsilon}_k$ associated with the bar element numbers identified in the set o . In practice, these measurements are collected using appropriate sensors such as strain gauges. Let p be the set that contains the bar element numbers where the stresses will be predicted. Herein, the set p is selected to be $p = \{1, \dots, N + 1\}$, i.e. it is assumed that stresses are predicted at all bar elements.

Results demonstrating the effectiveness of the proposed methodology are first presented for a five degree of freedom system ($N = 5$) shown in Figure 2. The nominal values of the nodal masses are $m_1 = m_5 = 21$ Kg, $m_2 = m_4 = 15$ Kg and $m_3 = 12$ Kg. A uniform distribution of the properties of the bar elements is assumed resulting in uniform stiffness $k_i = k_0$, $i = 1, \dots, N$. The nominal values of the stiffness properties are chosen so that $k_0 = E_0 A_0 / L_0$, where $E_0 = 2.1 \times 10^{11} \text{ N/m}^2$, $A_0 = \pi(0.0035)^2 \text{ m}^2$ and $L_0 = 0.3 \text{ m}$ are same for all bar elements. For the mass and bar properties selected, the nominal values of the natural frequencies of the five degree of freedom system are

110.0 Hz, 193.4 Hz and 277.0 Hz, 344.3 Hz, 425.3 Hz. The damping matrix C in the equations of motion (13) is chosen assuming that the system is classically damped. Specifically, the damping matrix C is selected so that the values of the modal damping ratios are 1% for all contributing modes. A single excitation is considered which is applied at node $\rho = 5$. The measured strain response time histories $\underline{y}_k = \underline{\varepsilon}_k^{(o)}$ at the bar elements identified by the set o are used to predict the stress response time histories at all bar elements identified in the set p using the proposed Kalman filter approach. These predictions depend on the values of the measurement noise covariance R in the Kalman filter formulation. Herein, the noise covariance matrix R is selected to be a diagonal matrix of the form $R = \eta^2 \text{diag}(\hat{Q}_{yy})$, where ε gives the level of the observation error and $\text{diag}(\hat{Q}_{yy})$ denotes the diagonal matrix formed from \hat{Q}_{yy} after setting the non-diagonal terms to zero. In the numerical results that follow, the values of $\eta = 0.1\%$ and $\eta = 10\%$ are used which corresponds to very small and relatively large observation errors, respectively.

The simulated measurements and the reference fatigue predictions are first obtained for the Type I white noise excitation. For demonstration purposes, comparison between the reference (exact) stress power spectral density (PSD) simulated by the model and the estimated PSD from the Kalman filter (KF) are given in Figure 4 for the bar elements $p = \{2, 4, 6\}$, assuming that the measured strains are at bar elements $o = \{1, 2\}$. Results are presented for the case of relatively large model error ($s_i = 5\%$) in Figures 4a-b at bar elements 2 and 4 and for the case of zero model error ($s_i = 0$) in Figures 4c-d at bar elements 4 and 6. It can be seen in Figure 4a for the case of relatively large model error that the estimated PSDs of the stress at the bar element 2, where measurements are available, almost coincides with the corresponding reference stress PSDs simulated by the model. At the bar element 4, where measurements are not available, there is a discrepancy between the estimated and reference (exact) stress PSDs as shown in Figure 4b. For the case of relatively large model error, the discrepancies observed in Figure 4b are mainly due to the fact that the nominal model used for PSDs predictions from the Kalman filter approach differs from

the reference model used to simulate the reference PSDs. The size of the discrepancies depends on the size of the model error. Specifically, these discrepancies are shown in Figure 4b for relatively large model error ($s_i = 5\%$) to be significantly higher than the discrepancies observed in Figure 4c for zero model error ($s_i = 0$). For zero model error, the discrepancies shown in Figure 4c and 4d for bar elements 4 and 6, respectively, are due to the estimation error associated with the Kalman filter. However, it should be noted that the predictions of the PSD from the Kalman filter approach are quite good, especially for the high amplitudes around the resonance peaks which mainly contribute to the fatigue process.

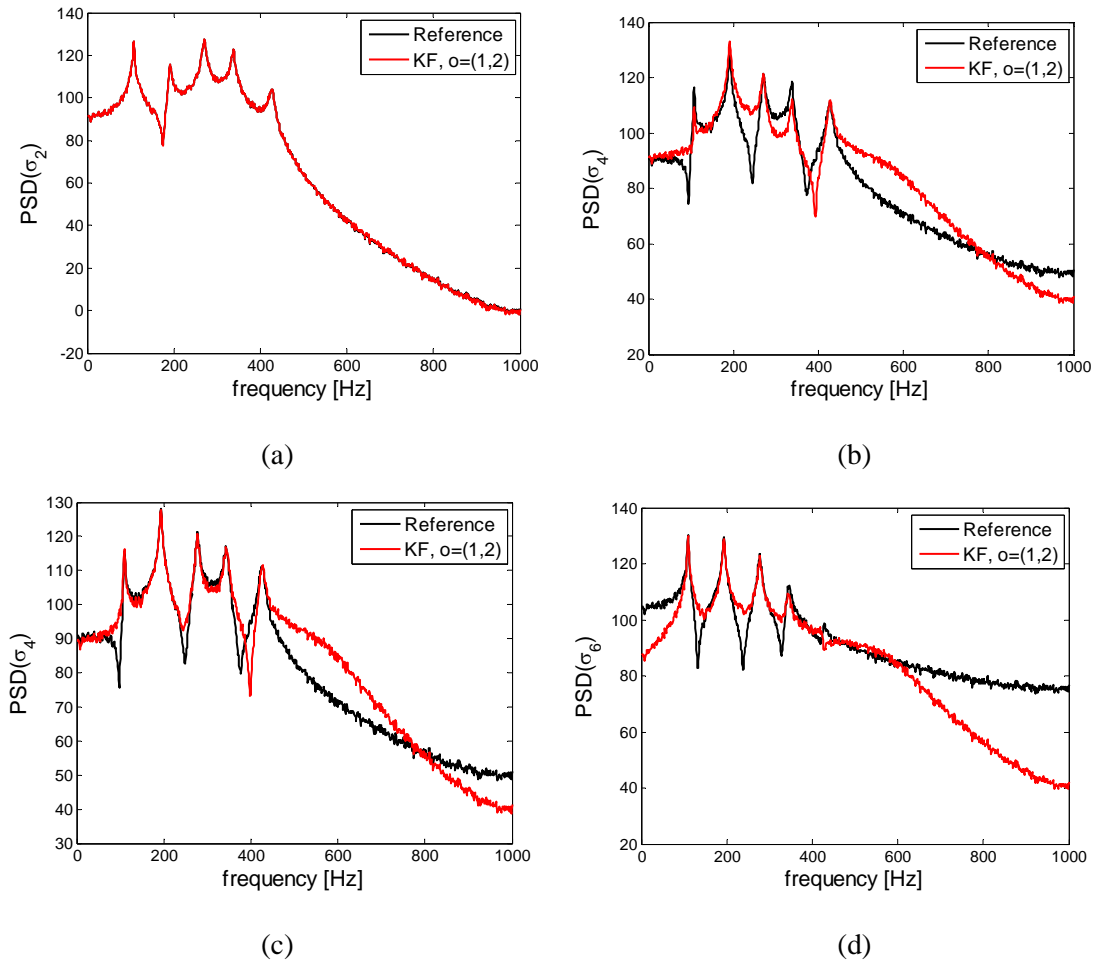


Fig. 4 Comparison between reference and estimated from Kalman filter PSD of the stress response at bar elements 2, 4 and 6; (a,b) relatively large model error $s = 5\%$, (c,d) zero model error $s = 0\%$.

Lifetime predictions due to fatigue are next compared in Figures 5a-d for all six bar (spring) elements of the structure. The lifetime values in these figures are obtained using the fatigue

prediction formula (5). For each bar element, there are six lifetime fatigue predictions. The first prediction is based on the reference time histories simulated by the reference model and it is used as the exact value against which to study the accuracy of the predictions from the proposed Kalman filter methodology. The other five fatigue-based lifetime estimates are the ones predicted by the methodologies based on the use of Kalman filter method and the nominal model to estimate the stress response time histories at all bar elements. To study the effect of the number and location of sensors on the accuracy of the predictions, the five fatigue lifetime estimates shown in Figures 5a to 5d correspond to the following five sensor configurations that differ from the number and location of sensors used: one sensor configuration $o = \{6\}$ involving one sensor placed at location or bar element 6, two sensor configurations $o = \{1,2\}$ and $o = \{3,4\}$ each one involving two sensors placed at locations denoted in the set o , and two sensor configurations $o = \{1,2,3\}$ and $o = \{2,3,4\}$ each one involving three sensors. In order to study the effect of model error on the accuracy of the Kalman filter methodology, the results in Figures 5a-c are based on simulated measurements from the reference model chosen to involve zero ($s_i = 0$), moderate ($s_i = 2\%$) and relatively large ($s_i = 5\%$) model error, while the observation error used for KF-based fatigue predictions is negligible ($\eta = 0.1\%$). In order to study the effect of observation error in the accuracy of the Kalman filter methodology, the results in Figure 5d are based on simulated measurements from the reference model chosen to involve zero model error ($s_i = 0$) and relatively large observation error ($\eta = 10\%$) used for KF-based fatigue predictions.

It can be seen from the results for the fatigue predictions involving zero model error ($s_i = 0$) shown in Figure 5a that the estimates based on the Kalman filter predictions are quite close to the reference fatigue values obtained from the actual (reference) response time histories. It also becomes clear that the accuracy of the Kalman filter predictions depend on the number and location of sensors in the structure. Specifically, the best predictions are obtained from one sensor placed at bar element 6. Similar accuracy in the predictions are obtained from the sensor configurations $o = \{3,4\}$ and $o = \{2,3,4\}$ involving two and three sensors. However, the sensor configurations

$o = \{1, 2\}$ and $o = \{1, 2, 3\}$ provide significantly less accurate predictions in the entire structure (all six bar elements) than the predictions provided by one sensor placed at location 6. Specifically, significant discrepancies between the reference and Kalman filter fatigue predictions from the sensor configurations $o = \{1, 2\}$ and $o = \{1, 2, 3\}$ are observed in bar element 5 and 6. It becomes evident from the results in Figure 5a that the locations and number of sensors affect the accuracy of the fatigue lifetime predictions from the proposed Kalman filter approach. Optimal sensor location methodologies [22] may be advantageously used to obtain the most informative locations that give the best accuracy in the fatigue lifetime predictions with the least number of sensors.

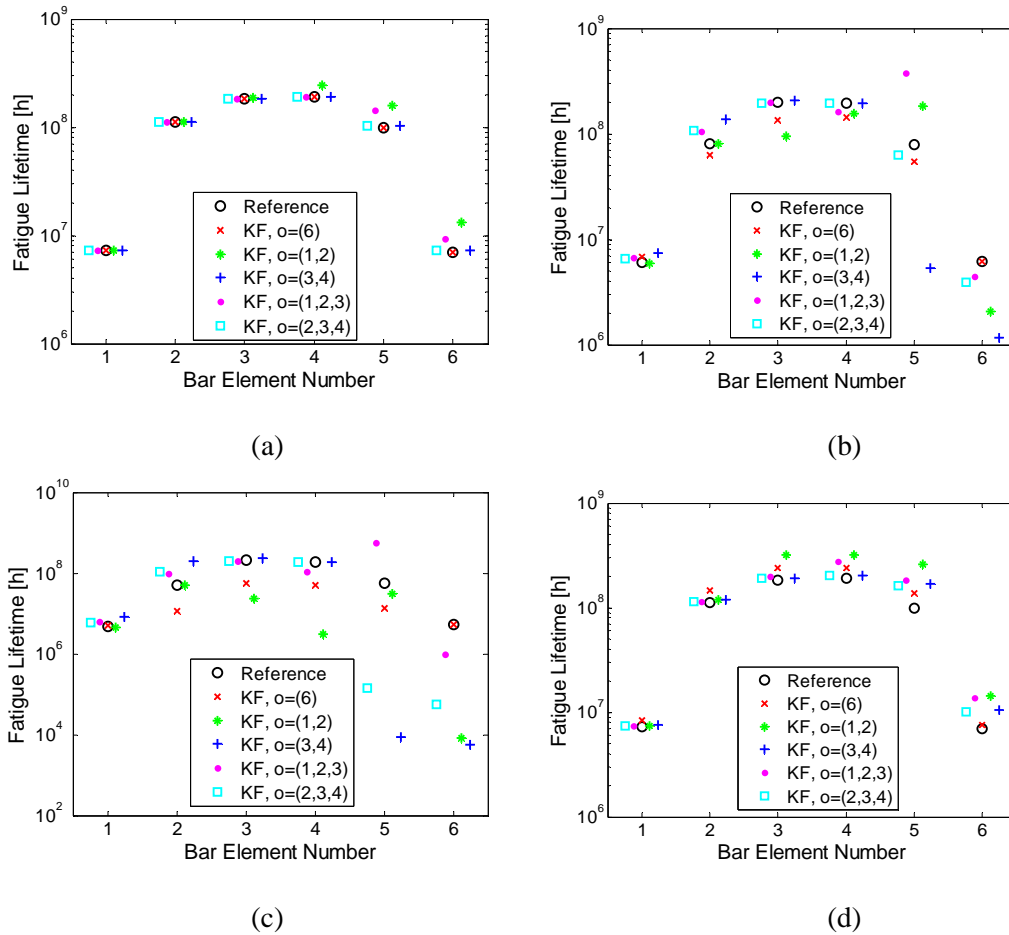


Fig. 5 Comparison of reference fatigue-based lifetime estimates and the estimates predicted by the Kalman filter for the $N = 5$ DOF model as a function of the number and location of sensors. (a) $s_i = 0$, $\eta = 0$, (b) $s_i = 2\%$, $\eta = 0$, (c) $s_i = 5\%$, $\eta = 0$, and (d) $s_i = 0$, $\eta = 10\%$.

Comparing the results in Figures 5a, 5b and 5c corresponding to zero ($s_i = 0$), moderate ($s_i = 2\%$) and larger ($s_i = 4\%$) model errors, it is evident that the size of model error affects the

accuracy of the fatigue prediction provided by the proposed Kalman filter methodology. For a fixed sensor configuration, the accuracy of the fatigue predictions obtained from the Kalman filter methodology deteriorates as the size of the model error increases. Moreover, the accuracy of the predictions depends highly on the number and location of sensors. There are optimal sensor locations which give the most accurate fatigue predictions. Specifically, the most accurate predictions in the entire structure for the case of moderate model error ($s_i = 2\%$) are obtained from sensor configurations $o = \{6\}$ and $o = \{2, 3, 4\}$ involving one and three sensors, respectively. For the case of larger model error ($s_i = 5\%$), the most accurate predictions in the entire structure (all bar elements) are obtained from sensor configurations $o = \{6\}$ involving one sensor, followed by the predictions provided by the sensor configuration $o = \{1, 2, 3\}$ involving three sensors.

The effect of measurement error on the fatigue predictions provided by the Kalman filter approach is next considered by comparing the results in Figure 5d obtained for relatively large observation error of the order of $\eta = 10\%$ with the results in Figures 5a-c obtained for very small ($\eta = 0.1\%$) observation error. It can be seen that the accuracy of the fatigue predictions is less sensitive to the magnitude of the observation error than it is to the magnitude of the model error. In addition, the accuracy of the fatigue lifetime predictions provided by the Kalman filter for the different sensor configurations observed in Figure 5d for zero model error and significant observation error ($\eta = 10\%$) does not significantly deteriorate as compared to the accuracy of the predictions observed in Figure 5a provided by the methodology for zero model error and very small ($\eta = 0.1\%$) observation error.

Next, results are also presented for simulated measurements generated from the Type II filtered white noise excitation. In this case, one examines the effect of the characteristics of the excitation on the accuracy of the proposed methodology. As before, the excitation is applied at node $\rho = 5$. Figure 6 compares the reference fatigue estimates and the fatigue predictions provided by the Kalman filter methodology for three different excitation characteristics: broadband excitation corresponding to values $\omega_f = 200\text{Hz}$ and $\zeta_f = 0.4$ (Figure 6a), and two lightly damped

excitations ($\zeta_f = 0.02$) with resonant frequencies close to the first, $\omega_f = \omega_1 \approx 110\text{Hz}$ (Figure 6b), and third $\omega_f = \omega_3 \approx 277\text{Hz}$ (Figure 6c), natural frequency of the structure. All results shown in Figures 6a-c are based on simulated measurements that involve zero model error ($s_i = 0$) and negligible measurement error $\eta = 0.1\%$. The results in Figure 6d are based on large model error ($s_i = 5\%$) and for the lightly damped excitation ($\zeta_f = 0.02$) with resonant frequency close to the third $\omega_f = \omega_3 \approx 277\text{Hz}$ natural frequency of the structure. All filtered white noise excitations correspond to the same variance. Given the values of ω_f and ζ_f , this is achieved by selecting appropriately the intensity of the white noise $n(t)$ so that the output $u(t)$ in (31) has the desired value of variance.

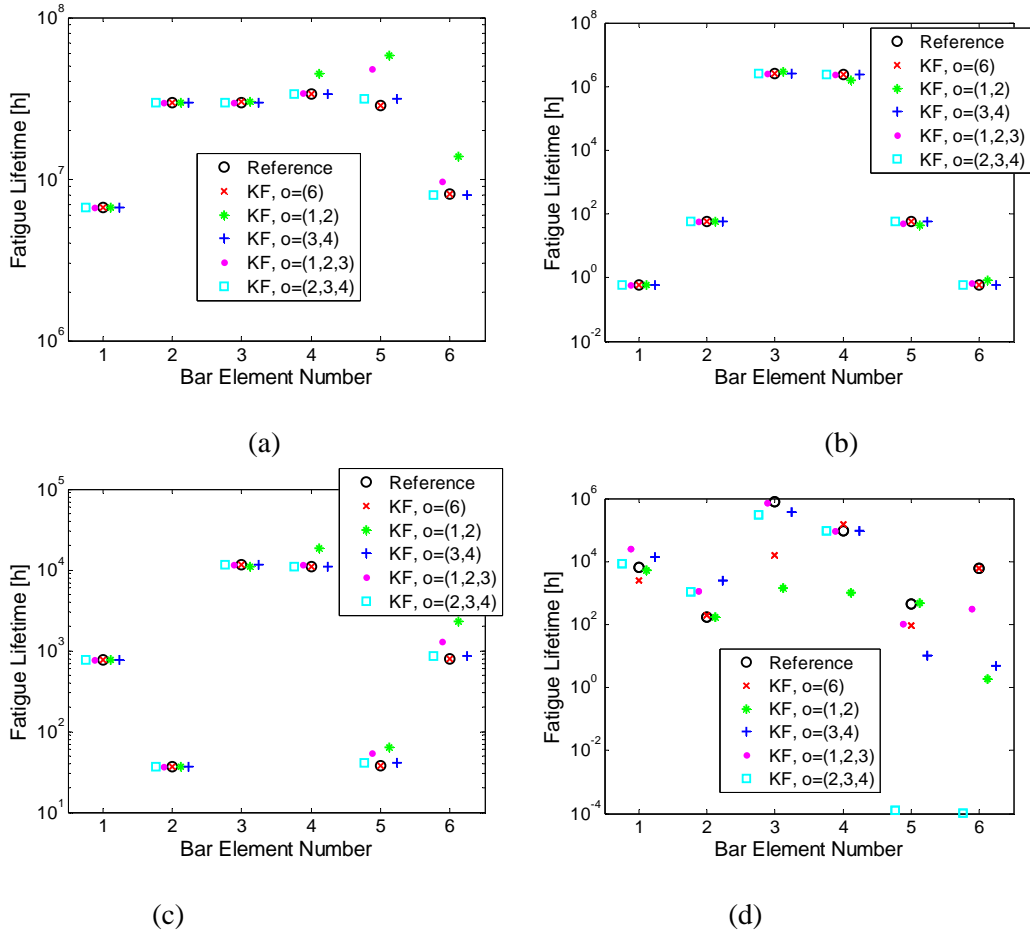


Fig. 6 Comparison of reference fatigue-based lifetime estimates and the estimates predicted by the Kalman filter for the $N = 5$ DOF model as a function of the number and location of sensors. (a) $\omega_f = 200\text{Hz}$, $\zeta_f = 0.4$, $s_i = 0$, (b) $\omega_f = \omega_1 \approx 110\text{Hz}$, $\zeta_f = 0.02$, $s_i = 0$, (c) $\omega_f = \omega_3 \approx 277\text{Hz}$, $\zeta_f = 0.02$, $s_i = 0$, and (d) $\omega_f = \omega_3 \approx 277\text{Hz}$ and $\zeta_f = 0.02$, $s_i = 5\%$.

It is clear in Figures 6a-c that for the case of zero model error the Kalman filter methodology gives very good predictions for a variety of excitation characteristics, including broad-band and lightly-damped excitations. As before, the accuracy of the predictions depends on the number and location of sensors. The most accurate predictions are obtained from the sensor configuration $o = \{6\}$ involving one sensor placed at location (bar element) 6, followed by the sensor configurations $o = \{3,4\}$ and $o = \{2,3,4\}$ involving two and three sensors. Less accurate predictions are obtained from the sensor configurations $o = \{1,2\}$ and $o = \{1,2,3\}$ involving two and three sensors, respectively. Obviously, optimizing the sensor placement in the structure can significantly improve the accuracy of the fatigue lifetime predictions provided by the Kalman filter methodology. Comparing the fatigue prediction results given in Figure 6d for large model error $s_i = 5\%$ to the fatigue prediction results in Figure 6c for zero model error, it is clear that the accuracy of the predictions from the Kalman filter methodology deteriorates as the model error increases. Sensor configuration $o = \{6\}$ involving one sensor provides predictions with the best accuracy compared to the predictions provided by all other sensor configurations used in Figure 6.

For the two lightly damped excitations shown in Figures 6b and 6c, it is observed that the fatigue at each bar element depends on the mode excited. For the excitation with dominant frequency close to the first natural frequency (Figure 6b), the structure responds mainly to its first mode and the strains levels due to vibration, depending on the derivatives of the modeshape, are higher at bar elements 1 and 6, while due to symmetry they are lower at the middle bar elements 3 and 4. Consequently, the bar elements 1 and 6 are expected to have significantly less fatigue lifetime while the middle bar elements 3 and 4 are expected to have high fatigue lifetime, which is consistent with the results observed in Figure 6b. For the excitation with dominant frequency close to the third natural frequency, the structure respond mainly with its third mode and therefore high strain values are expected also to occur at internal bar elements 2 and 5, while due to symmetry the strains at the middle elements 3 and 4 are expected to be small. This is consistent with the small fatigue lifetime values predicted for the bar elements 2 and 5, and the high fatigue lifetime values predicted for the middle bar elements 3 and 4, as shown in Figure 6c.

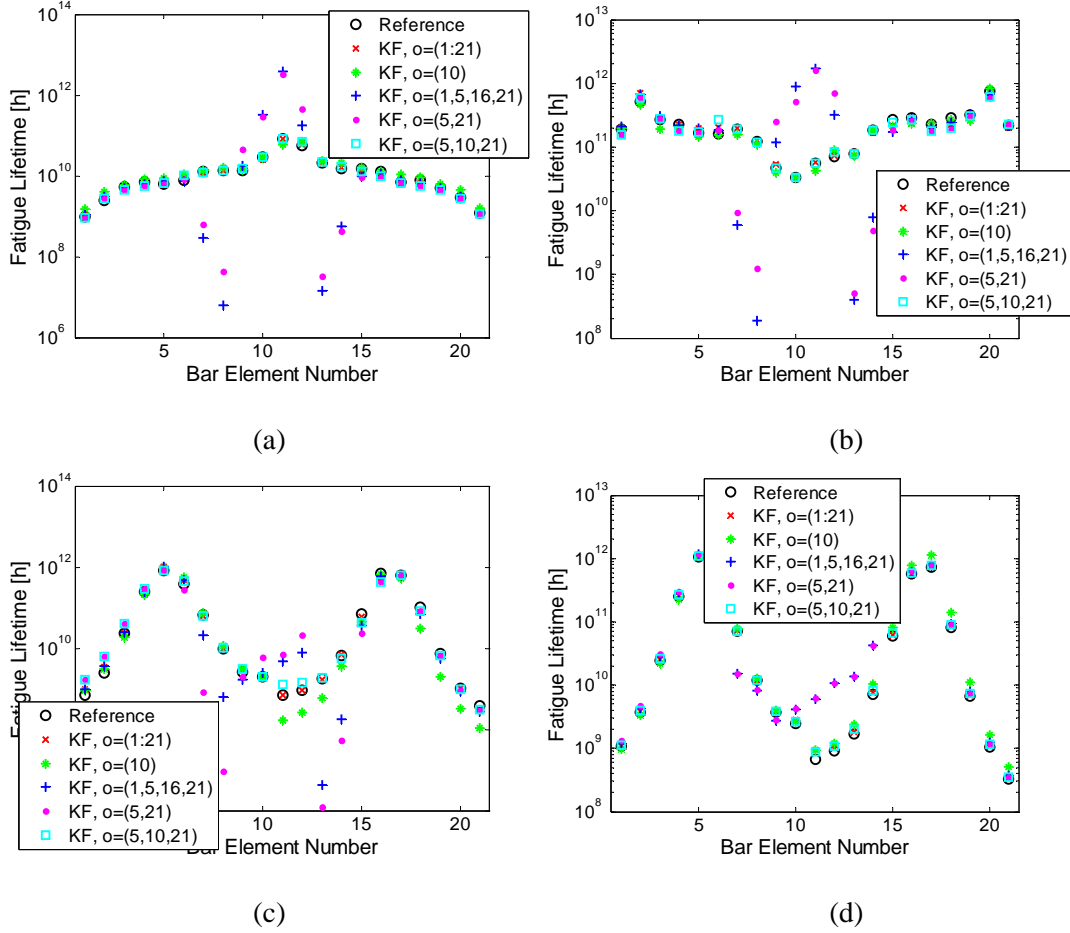


Fig. 7 Comparison of reference fatigue-based lifetime estimates and the estimates predicted by the Kalman filter for the $N = 20$ DOF model as a function of the number and location of sensors. (a) white noise, $s_i = 2\%$, $\eta = 0.1\%$, (b) $\omega_f = 110\text{Hz}$, $\zeta_f = 0.6$, $s_i = 2\%$, $\eta = 0.1\%$, (c) $\omega_f = \omega_2 \approx 44\text{Hz}$, $\zeta_f = 0.02$, $s_i = 2\%$, $\eta = 0.1\%$, (d) $\omega_f = \omega_2 \approx 44\text{Hz}$, $\zeta_f = 0.02$, $s_i = 0\%$, $\eta = 10\%$.

Finally, results demonstrating the effectiveness of the proposed methodology are presented for a twenty degree of freedom system ($N = 20$) shown in Figure 2. The nodal masses are assumed to be the same, i.e. $m_i = m_0$, $i = 1, \dots, N$. A uniform distribution of the properties of the bar elements is also assumed resulting in uniform stiffness $k_i = k_0$, $i = 1, \dots, N$. The nominal values of the mass and stiffness properties are chosen so that $m_0 = 30\text{Kg}$ and $k_0 = E_0 A_0 / L_0$, where $E_0 = 2.1 \times 10^{11} \text{N/m}^2$, $A_0 = \pi(0.0035)^2 \text{m}^2$ and $L_0 = 0.3\text{m}$ are same for all bar elements. For the mass and bar properties selected, the nominal values of the natural frequencies of the twenty degree of freedom system range from 22.5 Hz (minimum) to 300.8 Hz (maximum). The structure is

subjected to either Type I stationary white noise excitation or Type II non-white excitation applied at node $\rho = 10$, with constant spectral density matrix equal to $S_{\underline{u}} = S_0 = 10$. The strain response time histories $\underline{y}_k = \underline{\varepsilon}_k^{(o)}$ at the measured DOFs are used to predict the stress response time histories at all bar elements identified in the set $p = \{1, \dots, 21\}$ using the Kalman filter approach.

Lifetime predictions due to fatigue are shown in Figure 7 for all twenty one bar (spring) elements of the structure. For each bar element, there are six lifetime fatigue predictions. The first prediction is based on the reference time histories simulated by the reference model and it is used as the exact value against which to study the accuracy of the predictions from the proposed Kalman filter methodology. The second fatigue lifetime prediction is based on the use of Kalman filter method and the nominal model using sensors at all 21 bar elements. This second prediction uses measurements from all 21 bar elements and thus represents the most accurate results that can be obtained from the Kalman filter methodology. The other four fatigue-based lifetime estimates are the ones predicted by the methodologies based on the use of Kalman filter method and the nominal model to estimate the stress response time histories at all bar elements using a limited number of sensors. To study the effect of the number and location of sensors on the accuracy of the predictions, the four fatigue lifetime estimates shown in Figures 7a to 7d in the entire structure (all 21 bar elements) correspond to the following four sensor configurations that differ from the number and location of sensors used: one sensor configuration $o = \{10\}$ involving one sensor placed at location or bar element 10, one sensor configuration $o = \{5, 21\}$ involving two sensors placed at locations 5 and 21, one sensor configuration $o = \{5, 10, 21\}$ involving three sensors, and one sensor configuration $o = \{1, 5, 16, 21\}$ involving four sensors. Figure 7a compares results for white noise excitation, Figure 7b compares results for broadband filtered white noise excitation ($\omega_f = 110\text{Hz}$, $\zeta_f = 0.6$), while Figures 7c-d compare results for lightly damped filtered white noise excitations ($\zeta_f = 0.02$) with dominant frequency close to the second natural frequency of the structure ($\omega_f = \omega_2 \approx 44\text{Hz}$). Predictions in Figure 7a-c correspond to moderate model error ($s_i = 2\%$) and

very small observation error ($\eta = 0.1\%$). In order to study the effect of observation error in the accuracy of the Kalman filter methodology, predictions in Figure 7d correspond to zero model error ($s_i = 0\%$) and large observation error ($\eta = 10\%$).

It can be seen that despite the moderate model error considered in Figures 7a-c and the large measurement error considered in Figure 7d, the fatigue lifetime prediction values provided by the Kalman filter approach for a full sensor configuration involving 21 sensors installed in all 21 bar elements are quite close to the reference fatigue lifetime values. For given excitation case, it becomes clear that the accuracy of the fatigue lifetime predictions based on the Kalman filter approach using fewer than 21 sensors depend on the number and location of sensors in the structure. Specifically, the best predictions are obtained from the sensor configurations $o = \{10\}$ involving one sensor located at element 10 and the sensor configuration $o = \{5,10,21\}$ involving three sensors located at elements 5, 10 and 21. Such predictions are quite close to the reference fatigue values obtained from the actual (reference) response time histories and to the Kalman filter prediction provided by a full sensor configuration involving 21 sensors. It should be noted that the sensor configuration $o = \{5,10,21\}$ gives slightly better fatigue lifetime prediction accuracy at all 21 bar elements than the sensor configuration $o = \{10\}$. This is due to the fact that the sensor configuration $o = \{5,10,21\}$ contains the sensor configuration $o = \{10\}$ and in addition it involves two extra sensors that provide additional information for reconstructing more accurately the response at unmeasured locations. However, the sensor configurations $o = \{5,21\}$ and $o = \{1,5,16,21\}$ involving two and four sensors, respectively, provide significantly less accurate predictions, especially at the bar elements 7 to 14, than the predictions provided by the sensor configurations $o = \{10\}$ and $o = \{5,10,21\}$ involving one and three sensors, respectively. It thus becomes evident from the results in Figure 7 that the location and number of sensors affect the accuracy of the fatigue lifetime predictions. Optimal sensor location strategies [22] may be advantageously used to obtain the most informative locations that give the best accuracy in the fatigue lifetime predictions with the least number of sensors.

The relative importance of the model and measurement error on the accuracy of the fatigue predictions provided by the Kalman filter is investigated by comparing the results in Figure 7d obtained for relatively large observation error of the order of $\eta = 10\%$ and zero model error with the results in Figures 7c obtained for very small ($\eta = 0.1\%$) observation error and moderate model error ($s_i = 2\%$). It can be seen from these figures that the accuracy of the fatigue predictions are less sensitive to the size of the observation error. Specifically, the accuracy of the fatigue lifetime predictions provided by the Kalman filter for the different sensor configurations observed in Figure 7d for zero model error and significant observation error ($\eta = 10\%$) does not significantly deteriorate as compared to the accuracy of the predictions observed in Figure 7c provided by the methodology for moderate model error ($s_i = 2\%$) and very small observation error ($\eta = 0.1\%$).

5 CONCLUSIONS

A methodology for estimating damage due to fatigue on the entire body of a structure using spectral methods and output only vibration measurements at a limited number of locations was presented. The fatigue predictions presented in this work were illustrated for structural members subjected to a uni-axial stress state. These predictions can be extended using available methods [12-13] to structural members subjected to multi-axial stress state. Using the available response time history measurements and a model of the structure, a Kalman filter approach was used for predicting the power spectral densities of the stresses in the entire body of the structure needed in the spectral based fatigue prediction methodology. These power spectral density predictions were used to construct fatigue accumulation and lifetime prediction maps consistent with measurements provided by a monitoring system. Simulated measurements from a spring-mass chain-like structure suggest that the proposed methodology for lifetime fatigue prediction provide sufficiently accurate estimates even for the cases where the broadband assumptions of the stochastic excitation processes are violated. In particular, systematic numerical studies have demonstrated that the accuracy of the proposed methodology depend on the size of the model and observation errors, as well as the number and location of sensors.

The proposed method can also be seen as a tool for a life-time prognosis within structural health monitoring concepts. Specifically, the proposed method can be used to estimate the accumulation of damage due to fatigue during operation in the entire body of a structure taking into account the actual conditions collected from a sensor network placed at limited number of locations. The fatigue accumulation and lifetime predictions provided by the proposed methodology are useful for designing optimal maintenance strategies for most critical components of metallic structures using information collected from a sensor network.

ACKNOWLEDGMENTS

This research was funded by the Greek National Scholarship Foundation (IKY) within the IKYDA program framework and by the Deutscher Akademischer Austausch Dienst (DAAD, German Academic Exchange Service) within the PPP program. This research is also part of the 03-ED-524 project, implemented within the framework of the “Reinforcement Programme of Human Research Manpower” (PENED) and co-financed 25% from the Greek Ministry of Development (General Secretariat of Research and Technology) and 75% from E.U. (European Social Fund).

REFERENCES

- [1] A. Palmgren, Die Lebensdauer von Kugallagern, VDI-Zeitschrift, 68(14) (1924) 339-341.
- [2] M.A. Miner, Cumulative damage in fatigue, Applied Mechanics Transactions, ASME, 12(3) (1945) A159-A164.
- [3] L.D. Lutes, S. Sarkani, Random Vibrations: Analysis of Structural and Mechanical Systems, Elsevier Butterworth-Heinemann, 2004.
- [4] P.H. Wirsching, M.C. Light, Fatigue under wide band random stress, Journal of Structural Engineering, ASCE, 106(7) (1980) 1593-160.
- [5] L.D. Lutes, M. Corrao, S-L.J. Hu, J. Zimmerman, Stochastic fatigue damage accumulation, Journal of Structural Engineering, ASCE, 110(11) (1984) 2585-2601.
- [6] L.D. Lutes, C.E. Larsen, Improved spectral method for variable amplitude fatigue prediction, Journal of Structural Engineering, ASCE, 116(4) (1990) 1149-1164.

- [7] I. Rychlik, On the ‘narrow-band’ approximation for expected fatigue damage, *Probabilistic Engineering Mechanics*, 8 (1993) 1–4.
- [8] T. Dirlik, *Applications of Computers to Fatigue Analysis*, PhD Thesis, Warwick Univ., 1985.
- [9] D. Benasciutti, R. Tovo, Comparison of spectral methods for fatigue analysis of broad-band Gaussian random processes, *Probabilistic Engineering Mechanics*, 21 (2006) 287–299.
- [10] R.E. Kalman, R.S. Bucy, New results in linear filtering and prediction theory, *J. of Basic Eng., Trans. ASME, Series D*, 83(3) (1961) 95–108.
- [11] A. Preumont, V. Piefort, Predicting random high cycle fatigue life with finite elements, *ASME Journal of Vibration and Acoustics*, 16 (1994) 245–248.
- [12] B.R. You, S.B. Lee, A critical review on multiaxial fatigue assessments of metals, *International Journal of Fatigue*, 18(4) (1996) 235–44.
- [13] X. Pitoiset, A. Preumont, Spectral methods for multiaxial random fatigue analysis of metallic structures, *International Journal of Fatigue*, 22 (2000) 541–50.
- [14] S. Sarkani, D.P. Kihl, J.E. Beach, Fatigue of welded joints under narrowband non-Gaussian loadings, *Probabilistic Engineering Mechanics*, 9 (1994) 179-190.
- [15] X. Wang, J.Q. Sun, Multi-stage regression fatigue analysis of non-Gaussian stress processes, *Journal of Sound and Vibration*, 280 (2005) 455-465.
- [16] N.N.M. Bishop, F. Sherrat, A theoretical solution for the estimation of the rainflow ranges from power spectral density data, *Fatigue and Fracture of Engineering Materials and Structures*, 13(4) (1990) 311-326.
- [17] D. Benasciutti, R. Tovo, Spectral methods for lifetime prediction under wide-band stationary random processes, *International Journal of Fatigue*, 27 (2005) 867–877.
- [18] G.F. Franklin, J.D. Powell, M.L. Workman, *Digital Control of Dynamic Systems*, Second Edition, Addison-Wesley, 1990.
- [19] R.F. Stengel, *Stochastic Optimal Control: Theory and Applications*, John Wiley & Son, 1986.
- [20] P.D. Welch, The use of fast Fourier transform for the estimation of power spectra: a method based on time averaging over short, modified periodograms, *IEEE Trans. Audio Electroacoustics*, Vol. AU-15 (1967) 70-73.

- [21] M. Hayes, *Statistical Digital Signal Processing and Modeling*, John Wiley & Sons, 1996.
- [22] C. Papadimitriou, Optimal sensor placement methodology for parametric identification of structural systems, *Journal of Sound and Vibration*, 278(4) (2004) 923-947.

FIGURE CAPTIONS

Fig. 1 Scheme of life-time prediction from a limited number of sensors using a Kalman Filter.

Fig. 2 N -DOF spring mass chain-like model.

Fig. 3 Structure consisting of a series of N masses and $N + 1$ bar elements.

Fig. 4 Comparison between reference and estimated from Kalman filter PSD of the stress response at bar elements 2, 4 and 6; (a,b) relatively large model error $s = 5\%$, (c,d) zero model error $s = 0\%$.

Fig. 5 Comparison of reference fatigue-based lifetime estimates and the estimates predicted by the Kalman filter for the $N = 5$ DOF model as a function of the number and location of sensors. (a) $s_i = 0$, $\eta = 0$, (b) $s_i = 2\%$, $\eta = 0$, (c) $s_i = 5\%$, $\eta = 0$, and (d) $s_i = 0$, $\eta = 10\%$.

Fig. 6 Comparison of reference fatigue-based lifetime estimates and the estimates predicted by the Kalman filter for the $N = 5$ DOF model as a function of the number and location of sensors. (a) $\omega_f = 200\text{Hz}$, $\zeta_f = 0.4$, $s_i = 0$, (b) $\omega_f = \omega_1 \approx 110\text{Hz}$, $\zeta_f = 0.02$, $s_i = 0$, (c) $\omega_f = \omega_3 \approx 277\text{Hz}$, $\zeta_f = 0.02$, $s_i = 0$, and (d) $\omega_f = \omega_3 \approx 277\text{Hz}$ and $\zeta_f = 0.02$, $s_i = 5\%$.

Fig. 7 Comparison of reference fatigue-based lifetime estimates and the estimates predicted by the Kalman filter for the $N = 20$ DOF model as a function of the number and location of sensors. (a) white noise, $s_i = 2\%$, $\eta = 0.1\%$, (b) $\omega_f = 110\text{Hz}$, $\zeta_f = 0.6$, $s_i = 2\%$, $\eta = 0.1\%$, (c) $\omega_f = \omega_2 \approx 44\text{Hz}$, $\zeta_f = 0.02$, $s_i = 2\%$, $\eta = 0.1\%$, (d) $\omega_f = \omega_2 \approx 44\text{Hz}$, $\zeta_f = 0.02$, $s_i = 0\%$, $\eta = 10\%$.